High-spin yrast structure of ^{204}Hg from the decay of a four-hole, 22^{+} isomer

J. Wrzesiński, G. J. Lane, K. H. Maier, R. V. F. Janssens, G. D. Dracoulis, R. Broda, A. P. Byrne, M. P. Carpenter, R. M. Clark, M. Cromaz, B. Fornal, T. Lauritsen, A. O. Macchiavelli, M. Rejmund, B. Szpak, K. Vetter, and S. Zhu

Phys. Rev. C **92**, 044327 — Published 26 October 2015

DOI: 10.1103/PhysRevC.92.044327

High-spin yrast structure of ^{204}Hg from the decay of a four-hole, 22^+ isomer

J. Wrzesiński,[1] G. J. Lane,[2] K. H. Maier†,[1,2] R. V. F. Janssens,[3] G. D. Dracoulis†,[2] R. Broda,[1] A. P. Byrne,[2] M. P. Carpenter,[3] R. M. Clark,[4] M. Cromaz,[4] B. Fornal,[1] T. Lauritsen,[3] A. O. Macchiavelli,[4] M. Rejmund,[5] B. Szpak,[1] K. Vetter,[4] and S. Zhu[3]

[1] *The Niedwodniczański Institute of Nuclear Physics, PAN, Kraków PL 31-342, Poland*

[2] *Department of Nuclear Physics, Research School of Physical Sciences and Engineering, The Australian National University, Canberra ACT 0200, Australia*

[3] *Physics Division, Argonne National Laboratory, Argonne, IL 60439, USA*

[4] *Lawrence Berkeley National Laboratory, Berkeley, CA 94720, USA*

[5] *GANIL, BP 55076, 14076 Caen Cedex 5, France*

(Dated: September 15, 2015)

Abstract

A high-spin isomer with $\tau > 700$ ns has been found in ^{204}Hg, populated in reactions of 1360-MeV ^{208}Pb and 330-MeV ^{48}Ca beams with a thick ^{238}U target and a 1450-MeV ^{208}Pb beam on a thick ^{208}Pb target. The observed γ-ray decay of the isomer has established the yrast states below it, including another isomer with $\tau = 33(3)$ ns. The experimental results are compared with shell-model calculations that include four holes in the configuration space between ^{132}Sn and ^{208}Pb. The available spectroscopic information, including transition strengths, total conversion and angular correlation coefficients, together with the observed agreement with the calculations, allows spin, parity and configuration assignments to be proposed for the experimental states. The $\tau > 700$ ns isomer is the 22^+ state of maximum spin available from the alignment of the four valence holes with the configuration $\pi h_{11/2}^{-2} \nu i_{13/2}^{-2}$.

PACS numbers: 21.10.Tg, 21.60.Cs,23.20.Lv, 27.80.+w

I. INTRODUCTION

The study of high-spin isomers around ^{208}Pb has been crucial to the development of the nuclear shell model, providing information and experimental tests for calculations of detailed properties such as electromagnetic moments and transition strengths. The isomeric behaviour of excited states in near-closed shell nuclei often arises from their specific single-particle structure and/or low excitation energy. In certain nuclei with only a few particles or holes outside a closed shell, where the high-spin orbitals couple to the maximum or nearly maximum spin, there are often only a few possible configurations that can give rise to a state with a specific spin and parity. This can lead to clear configuration assignments and states with a rather simple structure that should be described well by the shell model. Hence, nucleon-nucleon residual interactions can be deduced, as well as transition matrix elements when state lifetimes are known. Such states often represent building blocks for the calculation and understanding of more complex multi-particle configurations.

Isomeric states also provide increased experimental sensitivity in non-selective reaction processes such as relativistic fragmentation [1], and deep-inelastic collisions (see, for example, Ref. [2] and references therein). Examples from the present studies, where isomers have provided the sensitivity required to study nuclei that are difficult to access, include the cases of ^{206}Hg [3] and ^{211}Pb [4]. Isomerism also enables the measurement of detailed properties such as electromagnetic moments [5].

The α-decaying state in ^{212}Po, with $T_{1/2}$= 45 s, was one of the first such cases of a high-spin, energy-favoured isomer. It was discovered by Perlman *et al.* [6] in 1962 at a time when α-particle spectroscopy of long-lived states was already well developed. Glendenning [7] explained that the unusually high α-decay hindrance was caused by the high spin of the isomeric state, suggesting an 18^+ assignment and an associated maximally-aligned, $\pi h_{9/2}^2 \nu i_{11/2}^2$ four-particle configuration. The absence of a γ-decay branch was understood by the state lying so low in excitation energy that the only possible γ-ray decay pathways were via low-energy, high-multipolarity transitions that are not favoured compared to α emission. Note that an alternative $\pi h_{9/2}^2 \nu g_{9/2} i_{11/2}$ configuration was suggested [8] for the isomer soon after the initial discovery, while an alternative 16^+ assignment, with the state arising from the $\pi h_{9/2}^2 \nu g_{9/2}^2$ coupling, was also postulated later to explain this long-lived state [9, 10]. It took some time before the 18^+ assignment with the $\pi h_{9/2}^2 \nu g_{9/2} i_{11/2}$ configuration was proven

indirectly by experiment [11]. The investigation of this isomer in ^{212}Po was arguably the beginning of the successful and still ongoing study of high-spin, shell-model isomers in this important region of the nuclear chart close to doubly-magic ^{208}Pb.

A corresponding, favoured high-spin state is also expected in ^{204}Hg, where,rather than four valence particles, four valence holes come into play. This level can be constructed from the highest spin two-hole states; e.g., the $\nu i_{13/2}^{-2}$ state coupled to $J^\pi = 12^+$ at 4027 keV in ^{206}Pb [12], and the two proton-hole $\pi h_{11/2}^{-2}$, 10^+ level at 3723 keV in ^{206}Hg [3].

The fact that ^{204}Hg is too neutron-rich to be reached by conventional (HI,xn) fusion-evaporation reactions accounts for the fact that only limited information on high-spin states is available thus far. The highest-spin state known is a 9^- level at 2723 keV observed [13] in an incomplete-fusion / inelastic-excitation reaction ^{204}Hg(^{9}Be,$\alpha\alpha n$). One more transition and a lifetime have been observed in fragmentation of a ^{208}Pb beam [14], but neither could be placed in the level scheme. Only recently have reaction and γ-spectroscopy methods been developed [2] that make it feasible to study neutron-rich nuclei at and beyond stability to high spins. The present work reports the observation of high-spin states in ^{204}Hg, taking advantage of time-correlated γ-ray spectroscopy to identify weakly populated isomers in deep-inelastic reactions between a ^{208}Pb beam and both ^{238}U and ^{208}Pb targets. These observations include the predicted 22^+ state. Computational methods have also been developed [15] to perform unrestricted shell-model calculations for the two-neutron and two-proton holes within the complete shell-model space between ^{132}Sn and ^{208}Pb for comparison with experiment, and this capability is taken advantage of here as well.

II. EXPERIMENTAL DETAILS

Data from four experiments have been combined to establish the high-spin level scheme of ^{204}Hg, each employing the general methods of thick-target γ-ray spectroscopy with deep inelastic reactions [2]. All experiments were performed at Argonne National Laboratory with beams from the ATLAS accelerator and used the Gammasphere [16] array with at least 100 Compton-suppressed, high-purity germanium detectors.

The first data are from a study with a beam of 1360-MeV ^{208}Pb ions incident on a 50 mg/cm^2, 100% enriched ^{238}U target (see, for example, Refs. [3, 4]), thick enough to stop all the reaction products. The beam was pulsed with $\sim$ 0.3 ns width and a repetition time

of 1.65 μs. Approximately 2.3 x 10^9 time-correlated γ-ray coincidence events were collected, comprising in-beam events with at least three suppressed γ rays in prompt coincidence and out-of-beam events requiring two or more Compton-suppressed γ rays. The correlated times and energies from the coincidence data collected using the ^{208}Pb + ^{238}U beam-target combination were input into a Blue database [17], subsequently enabling the efficient construction of coincidence matrices and cubes gated either by γ-ray energies, time with respect to the beam pulsing, or the relative time difference between the coincident γ rays.

In a second experiment with the same reaction, the distance between beam pulses was 412 ns. The emphasis in this case was more on prompt transitions.

The third experiment used a 330-MeV ^{48}Ca beam on a thick ^{238}U target (see, for example, Refs. [18, 19]) and also resulted in population of ^{204}Hg. Later, data from the reaction of 1450-MeV ^{208}Pb ions on a thick ^{208}Pb target with beam pulses separated by 412 ns were also available. While the results presented here are based mainly on data from the ^{208}Pb + ^{238}U experiment, the other data confirm and supplement the obtained assignments in some cases.

The fact that data from three different reactions with different beam pulsing conditions were available, facilitated the use of favourable, selective conditions to produce clean spectra and enable firm assignments of transitions and levels. A precise determination of the γ-ray intensities proved very helpful in this case, and was helped by the fact that these experiments produced many nuclei. As a result, a precise internal calibration of the energy-dependent efficiency was obtained by using a number of well-known isomeric and beta decays that could be matched to the energy range of interest, and could be combined with data from calibration sources. Close to 100 data points were determined for the fit of the efficiency curve. This methodology also accounts for the influence of both γ-ray self-absorption in the target and coincidence timing conditions. The efficiency curve in the crucial low-energy region is given in Fig.1 to demonstrate the precision achieved. The relative efficiency for lines in the low-energy region, which is very sensitive to details of the experimental setup (electronics and timing), was deduced from low-energy E1 and E2 transitions from the decay of known isomers in Sn, At, Hg, Os and Pb isotopes observed in the same experiment with the data normalized at higher energy to calibration points from sources.

The presence of a long-lived isomer at the top of the level scheme ensured that the alignment of the angular momentum of the nuclei produced in the reaction was lost for subsequent

γ-ray decays observed between the beam pulses. Therefore, angular correlations between pairs of γ-ray transitions were used to deduce transition multipolarities and infer changes in spin between consecutive levels. The ^{208}Pb+^{208}Pb experiment offered adequate statistics and, in most cases, a sufficiently low background level to determine angular correlation coefficients for many of the strong transitions.

III. EXPERIMENTAL RESULTS

The level scheme established from the experimental data is presented in the next section, while details about the spin and parity assignments are given in Sect. III B. Shell-model calculations are compared with the proposed level scheme in Sect. IV, and in some instances bring further support for the assignments.

A. The Level Scheme

The γ rays decaying from low-lying states up to the 3689-keV level were established by Poletti et al. [13]. The present data agree with these results, including the lifetime of the 7^- level. Coincidences relationships with these known lines were used to assign new γ rays in ^{204}Hg. The energies, level placements and prompt and delayed intensities for these transitions are presented in Table I and Fig. 2.

Coincidence spectra that display the main decay cascade are given in Fig. 3. Prominent new decays feeding the 3689-keV state are observed. The data indicate the presence of a cascade of transitions, from bottom to top, with energies of 598, 102, 536, 1127, parallel 253 and 205, and 921 keV. All of these lines are also observed out of beam (see Fig. 3(b)) and are, therefore, fed from an isomer.

The 921-keV γ ray exhibits no prompt (in-beam) component and is assigned as the decay from the top isomer. Only a lifetime limit of $\tau > 700$ ns could be deduced for this isomer because some of the experiments used only short beam pulse separations while, in the long-pulsing measurement with a beam burst separation of 1.65 μs, the composite dual/triple trigger condition caused time distortions.

The ordering of the other lines is mostly determined by their prompt/delayed intensity ratio, although a clear time-ordering of some transitions is made possible by the observation

(Fig. 6(b)) of another shorter-lived isomer with $\tau = 33(3)$ ns decaying via the 102-keV line.

Levels at 4287, 4389 (isomeric), 4925, 6052, 6305, and the long-lived isomer at 7226 keV are established from the main cascade. The 4287-keV state is verified by the presence of a 1563-keV crossover transition. A cascade of 136- and 991-keV γ rays is observed in parallel with the 1127-keV line, establishing another state at 5916 keV. The latter is also deexcited by a sequence of 792- and 736-keV transitions. The ordering of these two lines is not clear from the data, and the new intermediate level is placed at 5124 keV on the basis of a better match with theory (see Sect IV). The 6305-keV level is confirmed by a 1380-keV line to the 4925-keV state, while the 1237-keV γ ray establishes a new state at 6162 keV. The coincidence spectrum of Fig. 4, with coincidence gates that exclude the strong 109-keV transition, shows a weak 110-keV γ ray linking this level with the 6052-keV state. This weak line appears and is systematically present in all combinations of coincidence gates that include the 1134-keV line. It has the intensity expected for a highly-converted M1 transition. Possible contamination by the 108.9-keV transition in the spectrum was controlled through the absence of the 1062.4-keV line. Any transition other than the 110-keV one, which would account for the 30 units of missing intensity, was not observed. The presence of this transition is required to balance the intensity flowing through the complex parallel sequences immediately below the 6305-keV state.

From the coincidence relations, the 253-, 205-, and 110-keV decays are parallel to each other and they all populate the 6052-keV level. Assuming $M1$ multipolarities for these three transitions ($E2$ is also possible for the 253-keV line), their summed intensity balances that of the 921-keV isomeric decay and also the transitions below the 6052-keV level. This results in one additional level at 6258 keV depopulated by the 205-keV line and requires the presence of an unobserved 47-keV feeding transition, as proposed in Fig. 2. The intensity balance suggests that there is unobserved feeding for the 6126-keV state, presumably due to 95- or 142-keV transitions. However, taking into account the spin-parity assignments that will be discussed below, a 142-keV transition would be of $E2$ character and should have been observed when considering its lower conversion coefficient and higher detection efficiency compared to the possibility of a 95-keV, $M1$ transition. This favours the assignment of the 95-keV transition as the unobserved feeding of the 6162-keV state. This challenging region will be discussed further below.

Transitions feeding the long-lived state were isolated by projecting the prompt γ rays

observed in coincidence with delayed pairs of known transitions below the isomer. The insert in Fig. 3(a) and Fig. 5 present a sum of double-gated, prompt-delayed coincidence spectra. These provide evidence for four transitions located above the isomer; there is no indication that these γ rays are delayed. These high-energy transitions at 1945, 2071, 2195 and 2436 keV feed the isomer in parallel, and establish states at 9171, 9297, 9422 and 9662 keV, respectively.

B. Spin and Parity Assignments

In this section, the experimental data are used to assign spins and parities. The high statistics and clean spectra obtained from the decay of the long-lived isomer enabled the determination of total internal conversion coefficients, α_T, for several transitions based on intensity balance considerations. Results obtained for the ^{208}Pb+^{238}U experiment and the ^{208}Pb+^{208}Pb reaction are given in Table II. The multipolarity deduced from α_T coefficients, combined with the observed γ-ray branching ratios, and the yrast or near-yrast character expected for most levels, were important considerations in spin-parity assignments.

Since spin alignment is lost through the presence of the long-lived isomer, angular correlations were evaluated to provide information on the change of spin associated with each transition. For this purpose, the Gammasphere detectors were grouped in four sets with mean opening angles of 18.6°, 45.2°, 68.8° and 85.3°. Only double-coincidence events from the out-of-beam data with sufficient statistics were evaluated, although some intense combinations were obscured by background, notably the 598-keV line that is contaminated by neutron-induced background. Nevertheless, many pairs of transitions provided reliable results. These are presented in Table III where they are also compared with theoretical expectations for specific spin sequences. In Fig 7, examples of the measured angular correlations for various combinations of pairs of observed transitions indicate that the measured data are sufficient for the determination of values of the correlation coefficients. The presence of the short 33-ns isomer between the analyzed pairs of transitions does not appear to affect the observed correlations (e.g.; the 423-921-keV pair); presumably due to the cubic structure of the Pb target. The sign of the A_2 coefficient provides discrimination between $\Delta I = 1$ and $\Delta I = 2$ transitions. In the absence of a measurable lifetime, ΔI=2 behaviour generally implies $E2$ rather than $M2$ character and this assumption is used implicitly in a

number of cases below.

The total conversion coefficients, α_T (Table II), combined with the ΔI value obtained from angular correlations (Table III), support $E2$ assignments for the 436-, 423- and 692-keV transitions and confirm an $E1$ character for the 109-keV line, in agreement with the results of Poletti et al. [13] up to the 9^-, 2723-keV state.

The strong yrast cascade of 598- and 965-keV transitions dominates the decay from the 4287-keV level. The 965-keV line corresponds to a spin change of ΔI=2, as demonstrated by many angular correlations and, hence, the 3689-keV level has spin and parity 11^-. The small conversion coefficient for the 598-keV transition suggests an $E1$ or $E2$ assignment, with $E1$ being clearly favoured, resulting in a 12^+ assignment to the 4287-keV state resulting in the 1563-keV line being an $E3$ crossover. Above this state, the value of α_T=5.2(5) deduced for the 102-keV transition implies a clear $E2$ character and, hence, $I^\pi = 14^+$ for the isomer at 4389 keV. This assignment also provides a natural explanation for the 33-ns lifetime.

The higher cascade of transitions with energies of 536, 1127, 253, and 921 keV have respective values of $\Delta I = 2, 1, 2$, and 3 from the measured angular correlations. This implies $I^\pi = 16^+$ for the 4925-keV level, while the cascade of 1127- and 253-keV transitions, with a combined spin change of ΔI=3, results in $I = 19$ for the 6305-keV state. The lack of an observed lifetime implies that the 1380-keV crossover transition must be of $E3$ character. Hence, the states at 6305 and 6052 keV must have $I^\pi = 19^-$ and 17^-, respectively. Since the angular correlation of the 921-keV γ ray is more pronounced than is expected for a ΔI=2 transition, it implies an $E3$ multipolarity, establishing the 7226-keV level to have $I^\pi = 22^+$.

Returning to the complex region between 5916 and 6305 keV, the $E2$ character of the 253-keV transition forces the parallel 205- and 110-keV transitions to be of $M1$ multipolarity so as to balance the intensity depopulating the isomer. Then, the cascade between the 19^- and 17^- levels consisting of the 205-keV, $M1$ and unobserved 47-keV transitions implies an 18^- assignment for the intermediate 6258-keV state. Furthermore, all the states between 5916 and 6305 keV must have negative parity as they are connected by $M1$ or $E2$ transitions.

Firm spin assignments have now been proposed for all levels below the $\tau > 700$-ns isomer, except those at (5124), 5916 and 6162 keV. The cascade of the (unobserved) 95- and 1237-keV transitions connects an 18^- state to a 16^+ level via the 6162-keV level, while the cascade of 95- and 110-keV transitions connects 18^- and 17^- levels. The existence of the second cascade involving the 110-keV, $M1$ transition implies that the 95-keV line is also of $M1$

character and, hence, the 1237-keV γ ray must involve a change of parity. Excluding the $M2$ possibility, due to the absence of a lifetime, the 6162-keV state must have $I^\pi = 17^-$. The 5916-keV level is populated by the 136-keV γ ray feeding from a 17^- state. The measured conversion coefficient for this transition confirms $M1$ multipolarity and, hence, the 5916-keV state has $I^\pi = 16^-$ or 17^-, since 18^- is ruled out by the fact that the 991-keV transition would have to be of $M2$ multipolarity. A 17^- assignment would make this state yrast, whereas the 6052-keV, 17^- level is more strongly populated. Since yrast states are, in general, more favoured in deep-inelastic reactions [2], a 16^- assignment is preferred.

The order of the 792- and 736-keV decay cascade from the 5916-keV level is not clear from the measured intensities and, furthermore, the lack of spectroscopic information means that it is not possible to decide between 15^+, 16^+ or 15^- assignments for the intermediate (5124)-keV level. Nevertheless, as shown in Fig. 2, both the order of the transitions and the 15^+ assignment are favoured, based on comparisons with the results of the shell-model calculations presented in Sect. IV below.

Four transitions are observed to feed the 22^+ isomer, with the limited spectroscopic information preventing firm assignments of spins and parities. Note, however, that excitations of the collective octupole vibration of the ^{208}Pb core have been observed on top of many similar isomers in this region [20, 21]. The stretched-spin state, which would have $I^\pi = 25^-$ in this case, is usually yrast above the maximally-coupled isomeric states, with its excitation shifted from the 2615-keV energy observed in ^{208}Pb by the interaction involved in particle-vibration coupling. It has been observed that these shifts are additive [20] and the total shift in this case amounts to -483 keV from the constituent -212 keV and -271 keV shifts that have been observed for octupole excitations above the I^π=12^+ and 10^+ levels known in ^{206}Pb [12] and ^{206}Hg [3], respectively. The predicted transition energy, for a postulated 25^- state, is 2132 keV, which is 63 keV higher than the most intense feeding transition at 2195 keV. Hence, the 9422-keV level is the obvious candidate for this octupole-coupled state with $I^\pi = 25^-$, especially since the high intensity of this transition indicates its clear yrast character. Among the other three lines observed with much lower intensity, it is impossible to determine which correspond to non-stretched octupole couplings and which are associated with other excitations of the ^{208}Pb core.

IV. SHELL-MODEL CALCULATIONS AND COMPARISON WITH EXPERIMENT

A. Shell-Model Calculations and Spin Assignments

Shell-model calculations have been performed with the empirical interaction that was used earlier to satisfactorily reproduce the level schemes of ^{203}Hg [19] and ^{204}Tl [18]. The two lowest calculated states of each spin and parity are given in Fig. 8, beginning from $I^\pi = 5^-$, together with the observed decay pattern. Experimental and calculated levels are compared in Fig. 2, Fig. 8 and Table IV, with the latter also listing the two largest configuration components for all the states that have been assigned to an experimental counterpart. Note that the theoretical energies are not the usually calculated excitation energies obtained from the difference between the computed binding energies of the excited states and the ground state. Since the ground state consists of a rather complex configuration, when compared to that of high-spin states, calculation of its binding energy is less certain. As a result, the use of the precisely measured ^{204}Hg binding energy [22] is preferred with the 70-keV difference between data and calculation indicating that the computed ground state is somewhat less bound.

Shell-model calculations reproduce the pattern of the previously known 0^+, 2^+, 4^+ states [13], the close triplet of 6^+, 5^-, 7^- levels, and the 9^- state, all being clearly yrast. The calculated energies for the 2^+, 4^+, and 6^+ levels exhibit the largest deviations from experiment of around +200 keV. These states have heavily mixed configurations with the largest component corresponding to only $\sim$ 10% of the total wavefunction. The lowest calculated 11^- state is well separated in energy from other $I = 11$ levels and is a clear and unique match to experiment. The model then predicts a distinctive signature of closely spaced 12^+ and 14^+ levels (see Fig. 2), with the 102-keV, low-energy $E2$ transition between these states, providing a natural explanation for the lifetime of 33 ns (see Fig. 6). The shell model predicts low-lying 15^+ and 16^+ states above the 14^+ level that are a good fit with the observed 5124- and 4925-keV states, with both experiment and calculation agreeing that the 16^+ level is lower in energy. The 5124-keV level is then assigned $I^\pi = 15^+$ as no alternative is found in the calculations. Since the ordering of the 792- and 736-keV transitions is not known (see above), the 15^+ level might be at 5181 instead of 5124 keV. The calculation

placing the level at 4979 keV appears to favour the lower excitation energy, but is not decisive.

Proceeding to the top of the level scheme, the isomer at 7226 keV clearly corresponds to the fully-aligned $\pi h_{11/2}^{-2}\nu i_{13/2}^{-2}$ excitation expected from the maximal possible 22^+ coupling of the four valence holes. The large energy gap to the next higher levels at and above 9172 keV marks the transition to core-excited states and/or to coupling to an octupole vibration, as alluded to above. The 22^+ state can decay only to the two 19^- levels composed of the mixed configurations $\pi h_{11/2}^{-1}d_{3/2}^{-1} \otimes \nu i_{13/2}^{-2}$ and $\pi h_{11/2}^{-2} \otimes \nu i_{13/2}^{-1}f_{5/2}^{-1}$ (see Table IV). Therefore, the 6305-keV level is associated with the lower of those two predicted 19^- states, calculated at 6294 keV. Measured and calculated energies also agree well for the yrast 17^-, 6052-keV state and for the next lower level at 5916 keV with $I^\pi = 16^-$. Note especially that the high density of negative-parity states between 5916 and 6305 keV is predicted by the calculations.

In Fig. 8 it is apparent that the shell model provides a good overall description of the observed experimental energies, spins and parities, with all observed states having a corresponding computed level. Furthermore, there are no obvious states predicted by the calculations that have not been observed. The detailed agreement provides strong support for the proposed spin-parity assignment of 15^+ for the (5124)-keV state.

The average quadratic deviation between calculated and measured energies is only 69 keV for the states at and above the 5^- (see Table IV). The largest deviations are -146 and -130 keV for the 15^+ and 18^- levels, respectively. Both have a strong component of the $s_{1/2}$ and $h_{11/2}$ proton holes coupled to 6^-, for which the interaction energy is not well known. The energy of the second 17^- is also not calculated as well as that of other states. Nevertheless, the overall agreement is satisfactory, providing confidence in the proposed assignments.

B. Lifetimes and γ-ray transition strengths

This section compares the observed lifetimes, transition strengths and transition intensity ratios with expectations based on the spin assignments and the shell-model configurations discussed above.

12^+ decay: The two main components of the wavefunctions of the 12^+ state and the 11^- and 9^- levels to which it decays are so different that any γ-ray transition is forbidden. Note first that $E1$ transitions are forbidden within one major shell. Furthermore, $E3$ transitions

can only proceed from $\pi h_{11/2}^{-1}$ or $\nu i_{13/2}^{-1}$ orbitals to the high-lying $\pi d_{5/2}^{-1}$ or $\nu f_{7/2}^{-1}$ states that are only present with small admixtures of around 1% [19] in the final state. On the other hand, these transitions are fast, with $B(E3) \sim 25$ W.u., due to admixtures of the collective octupole vibration. Hence, a final $B(E3)$ of the order of 0.1 W.u. might be expected. The lifetime of the 12^+ state is limited by experiment to τ <5 ns and this, taken together with the measured γ-ray branching ratio of 1% between the 1564- and 598-keV transitions, leads to experimental strength limits of $B(E1) > 2.6 \times 10^{-7}$ W.u. and $B(E3) > 0.05$ W.u., both of which are plausible based on the computed wavefunctions.

14^+ decay: The $14^+ \rightarrow 12^+$ transition has a strength of $B(E2) = 5.2(3)$ W.u. This is an allowed decay according to the main configurations calculated for the 14^+ and 12^+ states involved and the magnitude of the transition strength appears to be reasonable.

19^- decay: At first glance, it seems rather implausible that the 253-keV ($E2$), and especially the 1380-keV ($E3$), transitions can compete with the $19^- \rightarrow 18^-$, $M1$ decay. Deducing the intensity of this 47-keV, $M1$ transition from the intensity balance with the 205-, 1237- and 110-keV γ rays and using the experimental lifetime limit of $\tau < 5$ ns, the implied transition strengths are $B(E3;\ 1380\ \text{keV}) > 0.12$ W.u., $B(E2;\ 253\ \text{keV}) > 0.23$ W.u. and $B(M1;\ 47\ \text{keV}) > 0.0027$ W.u. The limits on the $E3$ and $E2$ strengths are similar and plausible, so the main issue is whether the $M1$ transition can conceivably be suppressed by some orders of magnitude.

For both the 18^- and 19^- states, the two largest configuration components amount to >90% of the wavefunction (see Table IV). Only the second $\pi d_{3/2}^{-1} h_{11/2}^{-1} \otimes \nu i_{13/2}^{-2}$ component of the 19^- level can contribute to the $M1$ transition between them. The main transition element is to the same component of the 18^- state. In the 18^- wavefunction, the proton component $d_{3/2}^{-1} h_{11/2}^{-1}$ can couple to either 6 or $7\hbar$. The amplitudes, including the signs of these two components of the wavefunction, can be calculated with the code SESAME [23] since no configuration mixing is involved. This results in two transitions that interfere destructively and give a small, negative transition element. While it is possible that the magnitudes of the amplitudes are incorrect, the sign, and therefore the crucial destructive interference, is rather certain.

The third possible component of the $M1$ transition is to the $\pi s_{1/2}^{-1} h_{11/2}^{-1} \otimes \nu i_{13/2}^{-2}$ part of the 18^- state with the weak, spin-flip transition from $d_{3/2}^{-1}$ to $s_{1/2}^{-1}$. This component can contribute constructively or destructively, as only the square of its amplitude is known.

With the configuration probabilities given in Table IV, the $B(M1)$ strength is either 0.004 or 0.02 W.u., in agreement with the experimental limit. Furthermore, these values are some orders of magnitude less than the experimental limit on the $E2$ and $E3$ transitions, hence accounting for the initially unexpected intensity of the $E2$ and $E3$ transitions.

Note, also, that the calculated wavefunctions predict that the $19^- \rightarrow 16^+$, $E3$ transition can proceed through the strong $h_{11/2}^{-1}$ to $d_{5/2}^{-1}$ transition with a probability of 2% resulting in a strength of $B(E3) = 0.5$ W.u., again in agreement with the experimental limits.

15^+ to 18^- region: The 18^- level decays via $M1$ transitions to the two 17^- states, as might be naively expected, and not by an $E2$ decay to the 16^- state. A more detailed analysis to account for the observation is prohibitively complex.

The decay of the two 17^- levels does not obviously agree with the calculated main configurations in Table IV. The higher 17^- state would be expected to decay to the 16^- level rather than to the lower 17^- state. There is again the possibility that the transition elements might interfere destructively. Since $E1$ transitions are also observed to decay from both states, this may be an indication that the $M1$ transitions are weak and, therefore, unreliably predicted.

The 16^- state can only decay to positive-parity levels and two $E1$ transitions to the 15^+ and 16^+ states are observed in the experiment. Finally, the 15^+ and 16^+ levels decay to the 14^+ state, as allowed by strong components of the wavefunctions. A 15^+ to 16^+ branch would also be allowed, but is not observed, likely because of its low energy relative to the competing 736-keV transition.

22^+ decay: The decay from the 22^+ isomer proceeds through a single transition of 921 keV to the 19^- level with the parent state having a lifetime, $\tau > 700$ ns. This 22^+ level has a configuration with a single, unique component: the stretched $\pi h_{11/2}^{-2} \otimes \nu i_{13/2}^{-2}$ coupling. The two stretched configurations, $\pi h_{11/2}^{-2} \otimes \nu i_{13/2}^{-1} f_{5/2}^{-1}$ and $\pi h_{11/2}^{-1} d_{3/2}^{-1} \otimes \nu i_{13/2}^{-2}$, result in two 19^- states with orthogonal mixtures of these two components. The calculations in Table IV predict equal probabilities for both of these components and an energy difference of 245 keV. From the calculated wavefunctions it is expected that $E3$, $22^+ \rightarrow 19^-$ transitions can occur only between the $(h_{11/2}^{-2}; 10^+)$ and $(h_{11/2}^{-1} d_{3/2}^{-1}; 7^-)$ components, due to small $h_{11/2}^{-1} d_{5/2}^{-1}$ admixtures in the lower state, and between the $(i_{13/2}^{-2}; 12^+)$ and $(i_{13/2}^{-1} f_{5/2}^{-1}; 9^-)$ components through the admixture of the $i_{13/2}^{-1} f_{7/2}^{-1}$ configuration. The strength of these types of $E3$ transitions has been measured directly through observation of the $10^+ \rightarrow 7^-$ and $12^+ \rightarrow 9^-$ transitions in ^{206}Hg

and ^{206}Pb, respectively. In the present case, the results are strengths of $B(E3) = 0.76$ W.u. and $B(E3) = 0.02$ W.u. for constructive and destructive interference, respectively. Both of these values are less than the experimental strength limit of $B(E3) < 1.77$ W.u. Furthermore, the relative intensity of the unobserved branch to the upper level, assuming that it corresponds to the branch with destructive interference and accounting for the calculated energy difference of 245 keV, is then 0.2 in the intensity units of Table I, consistent with the non-observation of the latter branch in the experiment. Finally, an $E3$ strength of 0.76 W.u. for the 921-keV transition would give a predicted lifetime for the 22^+ state of $\tau = 1.6$ μs, sufficiently short to enable the observation of coincidence relationships across the isomer, while being consistent with the measured lifetime limit of $\tau > 700$ ns.

V. DISCUSSION AND CONCLUSIONS

From the precise transition intensity determination made possible by observing the decay of the 22^+ isomer in ^{204}Hg out-of-beam, accurate total conversion coefficients and angular correlation coefficients could be obtained. Together with the observation of crossover transitions at the 1% intensity level, this has enabled spins and parities to be confirmed for all but one of the states below the 22^+ isomer, strictly from experiment. For the remaining level, the shell model suggests a unique assignment.

Besides ^{204}Hg, the yrast lines of ^{203}Hg, ^{204}Tl and ^{205}Tl have also been studied by γ-ray spectroscopy with deep-inelastic reactions [18, 19, 21]. The shell-model structure of all of these nuclei is determined by neutron and proton holes in the ^{208}Pb core. The yrast line is distinctively shaped by the $\nu i_{13/2}^{-1}$ and $\pi h_{11/2}^{-1}$ intruder orbitals with opposite parity and $4\hbar$ more angular momentum than the lower-energy neutron $(p_{1/2}, f_{5/2}, p_{3/2})$ and proton $(s_{1/2}, d_{3/2})$ states. Therefore, when an additional hole is moved into an intruder level, the parity changes. Figure 8 indicates that this occurs regularly with each increase of 4 to $6\hbar$ along the yrast line. In the ~ 2 MeV intervals between these parity changes, the holes in the natural-parity orbitals couple successively to higher angular momentum. This pattern establishes a clear structure evident for all four ^{203}Hg, ^{204}Hg, ^{204}Tl, and ^{205}Tl nuclei where, within each group of equal parity states $M1$ and $E2$ transitions prevail, while a parity-changing $E1$ or, often, $E3$ transition, separates each group.

The binding energies relative to ^{208}Pb in all four nuclei are remarkably well reproduced for

the high-spin states with a deviation lower than 40 keV. The two-body interaction energies between the $\pi h_{11/2}^{-1}$ and $\nu i_{13/2}^{-1}$ hole in the 10^- and 11^- states have been deduced from the experimental levels in ^{204}Tl and ^{205}Tl, so that the agreement for these two nuclei is somewhat artificial. But for ^{203}Hg and ^{204}Hg, all the matrix elements were taken from other nuclei and, in these cases, the ground states and all the other yrast levels are well reproduced. Table V summarizes the difference between calculated and measured binding energies for the ground states and unique high-spin isomers in each nucleus. As the mass of ^{206}Hg has an error of 20 keV, all proton-hole - proton-hole matrix elements are subject to this uncertainty. Accounting for this, the agreement for the high-spin isomers is nearly perfect.

In conclusion, in all four nuclei, including also the new results obtained for ^{204}Hg, the yrast structure has been established up to the highest spin that can be formed from the valence holes in the ^{208}Pb core. The observations are all in good agreement with shell-model predictions. In particular, the four-hole counterpart to the four-particle isomer in ^{212}Po has now been found after 50 years of research.

ACKNOWLEDGMENTS

This work is supported by Australian Research Council (FT100100991) and the United States Department of Energy, Office of Science, Office of Nuclear Physics, under contract numbers DE-AC02-06CH11357 and DE-AC02-05CH11231. This research used resources of ANL's ATLAS facility, which is a DOE Office of Science User Facility.

[1] M. Caamano *et al.*, Eur. Phys. J. A **23**, 201 (2005).

[2] R. Broda, J. Phys. G **32**, R151 (2006).

[3] B. Fornal *et al.*, Phys. Rev. Lett. **87**, 212501 (2001).

[4] G. J. Lane *et al.*, Phys. Lett. B **606**, 34 (2005).

[5] G. Neyens, Rep. Prog. Phys. **66**, 633 (2003).

[6] I. Perlman, F. Asaro, A. Ghiorso, A. Larsh, and R. Latimer, Phys. Rev. **127**, 917 (1962).

[7] N. K. Glendenning, Phys. Rev. **127**, 923 (1962).

[8] N. K. Glendenning and K. Harada, Nucl. Phys. **72**, 481 (1965).

[9] D. Strottman, Phys. Rev. C **20**, 1150 (1979).

[10] N. Auerbach and I. Talmi, Phys. Lett. **10**, 297 (1964).

[11] A. R. Poletti, G. D. Dracoulis, A. P. Byrne, and A. E. Stuchbery, Nucl. Phys. **A473**, 595 (1987).

[12] J. Blomqvist, R. Liotta, L. O. Norlin,U. Rosengård, B. Fant, T. Weckström1, H. C. Jain, T. Lönnroth, Nucl. Phys. **A554**, 45 (1993).

[13] A. R. Poletti, G. D. Dracoulis, A. P. Byrne, A. E. Stuchbery, B. Fabricius, T. Kibedi, and P. M. Davidson, Nucl. Phys. **A580**, 64 (1994).

[14] S. J. Steer *et al.*, Phys. Rev. C **84**, 044313 (2011).

[15] B. A. Brown *et al.*, The computer code OXBASH, MSU-NSCL Report Nr. 524.

[16] I. Lee, Nucl. Phys. A **520**, 641c (1990) and http://www.phy.anl.gov/gammasphere/

[17] M. Cromaz, T. J. M. Symons, G. J. Lane, I. Y. Lee, and R. W. MacLeod, Nucl. Instr. Meth. Phys. Res. A **462**, 519 (2001).

[18] R. Broda *et al.*, Phys. Rev. C **84**, 014330 (2011).

[19] B. Szpak *et al.*, Phys. Rev. C **83**, 064315 (2011).

[20] M. Rejmund *et al.*, Eur. Phys. J. A **8**, 161 (2000).

[21] J. Wrzesinski *et al.*, Eur. Phys. J. A **20**, 57 (2004).

[22] G. Audi, A. H. Wapstra and C. Thibault Nucl. Phys. **A729**, 337 (2003).

[23] P. M. Davidson, University of Auckland, MSc thesis (1990), unpublished.

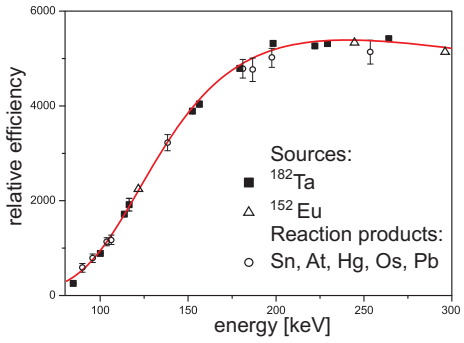

FIG. 1. Relative γ-ray efficiency calibration for the low-energy range in the ^{208}Pb+^{208}Pb experiment; the open circles are the calibration points for transitions from the decay of known isomers in Sn, At, Hg, Os, Pb isotopes populated in the experiment with the data normalized at higher energy to calibration points from sources.

TABLE I. Energies and intensities of γ-ray transitions observed in the measurements with the ^{208}Pb+^{238}U and ^{208}Pb+^{208}Pb reactions, together with deduced levels in ^{204}Hg. Multipolarities are assigned from the combined results of total conversion coefficients in Table II and angular correlations in Table III.

Initial level		Transition	Final	$X\lambda$	^{208}Pb + ^{238}U		^{208}Pb + ^{208}Pb	
E	J^π	E_γ	level		I_γ		I_γ	
(keV)	[h]	(keV)	(keV)		in-beam[a]	off-beam[b]	in-beam[a]	off-beam[b]
0	0^+							
436.56	2^+	436.56 (3)	0	E2		94 (4)		96 (1)
1128.38	4^+	691.82 (3)	436.6	E2		99 (3)		99 (1)
2190.79	6^+	1062.41 (3)	1128.4		61 (3)	67 (3)	63 (2)	69 (1)
2262.76	5^-	1134.38 (3)	1128.4		35 (2)	27 (2)	33 (1)	27 (1)
2299.66	7^-	36.9[d]	2262.8					
		108.90 (5)	2190.8	E1	37 (3)	61 (3)	31 (2)	51 (2)
		1171.26 (7)	1128.4		4 (1)	5.8 (8)	4.1 (4)	5.7 (3)
2723.31	9^-	423.65 (3)	2299.7	E2	47 (2)	97 (4)	53 (1)	96 (1)
3688.56	11^-	965.25 (4)	2723.3	E2	21 (2)	94 (2)	28 (1)	97 (1)
4286.91	12^+	598.34 (3)	3688.6	E1	19 (2)	99 (2)	25 (1)	99 (1)
		1563.5 (2)	2723.3				0.4 (1)	1.0 (2)
4388.7	14^+	101.8 (1)	4286.9	E2		20 (3)	1.6 (5)	16 (1)
4924.8	16^+	536.12 (5)	4388.7	E2	4 (2)	89 (4)	4.4 (1)	89 (2)
5124.4[g]	15^+	735.7 (1)	4388.7			7.1 (6)	0.4 (1)	8.0 (6)
5916.2	16^-	991.34 (9)	4924.8			13 (2)	1.1 (2)	9.9 (10)
		791.8 (2)	5124.4			9.4 11)	0.4 (2)	7.4 (8)
6052.2	17^-	1127.34 (3)	4924.8		2 (1)	78 (3)	2.6 (2)	79 (2)
		136.4 (4)	5916.2	M1		3.8 (7)	0.6 (2)	4.8 (6)
6162.3	17^-	1237.5 (1)	4924.8			3.9 (5)	1.1 (3)	3.9 (3)
		110.0 (5)	6052.2	(M1)[f]		[c]		5 (2)
6257.7	18^-	95[d]	6162.3					
		205.5 (1)	6052.2	(M1)[f]		17 (3)		22 (2)
6305.1	19^-	47[d]	6257.7					
		252.9 (1)	6052.2	(E2)[f]		16 (3)	0.5 (1)	15 (2)
		1380.1 (2)	4924.8			1.8 (6)		1.1 (1)
7226.1	22^+	921.03 (5)	6305.1			95 (4)		91 (3)
9170.9		1944.8 (5)	7226.1		16 (4)[e]		11 (2)[e]	
9297.0		2070.9 (4)	7226.1		14 (4)[e]		14 (2)[e]	
9421.6	(25^-)	2195.5 (2)	7226.1		100 (9)[e]		100 (8)[e]	
9662.1		2436.0 (2)	7226.1		37 (6)[e]		38 (5)[e]	

[a] In-beam relative intensities are determined from the prompt spectrum double-gated on the 436.6- and 691.8-keV transitions. 100 unit of relative intensity represents the sum of 1062.4-, 1171.3- and 1134.4-keV lines feeding the 4^+state.

[b] Out-of-beam relative intensities are normalized to 100 decays of the 7226-keV isomer.

[c] Contaminated line with intensity not determined.

[d] Transition energy inferred from coincidence relationships, but not observed directly.

[e] Relative intensities have been estimated from coincidence spectra looking early in time across the isomeric state at 7226 keV.

[f] The proposed multipolarities for these three transitions are the best (optimal) combination to balance the intensity from the isomer (see text).

TABLE II. Total electron conversion coefficients, α_T, extracted based on intensity balance considerations in the ^{208}Pb+^{238}U and ^{208}Pb+^{208}Pb reactions, are compared with expected values and the values of ΔI deduced from angular correlation measurements (from Table III). The resulting transition multipolarities are listed in column 7.

E_γ	α_T		α_T (expected values)			$X\lambda$	ΔI
(keV)	^{208}Pb + ^{238}U	^{208}Pb + ^{208}Pb	$E1$	$M1$	$E2$		
101.8	3.8 (9)	5.2 (5)	0.4041	7.503	5.144	$E2$	
108.9	0.11 (6)	0.37 (7)	0.3412	6.186	3.888	$E1$	1
136.4	4.6 (12)	2.7 (5)	0.1933	3.253	1.582	$M1$	
423.6		0.03 (2)	0.0127	0.1423	0.0408	$(E1, E2)$	2
436.6	0.07 (4)	0.05 (2)	0.0119	0.1313	0.0378	$E2$	2
536.1	0.08 (6)	0.06 (3)	0.0077	0.0763	0.0228	$(E2, M1)$	2
598.3		< 0.01	0.0061	0.0573	0.0177	$E1$	
691.8		0.018 (20)	0.0046	0.0393	0.0128	$(E1, E2)$	2
965.2		0.02 (2)	0.0025	0.0167	0.0065		2

TABLE III. Angular correlation coefficients obtained in the ^{208}Pb+^{208}Pb experiment. Values for A_2 and A_4 coefficients obtained from fitting the extracted correlations for various transition pairs are compared with calculated values for the proposed spin assignments.

$(E_\gamma)_1$	$(E_\gamma)_2$	experiment		spin assignments				theory	
(keV)	(keV)	A_2	A_4	$(I_i)_1 \rightarrow (I_f)_1$		$(I_i)_2 \rightarrow (I_f)_2$		A_2	A_4
423.6	108.9	-0.10(3)	-0.27(5)	9	7	7	6	-0.11	0
”	436.6	0.12(2)	-0.05(3)			2	0	0.16	0.05
”	921.0	0.19(3)	-0.01(4)			22	19	0.19	-0.01
436.6	108.9	-0.08(3)	0.06(4)	2	0	7	6	-0.11	0
”	423.6	0.11(4)	-0.02(4)			9	7	0.16	0.05
”	598.3	[a]				12	11		
”	691.8	0.10(2)	-0.03(3)			4	2	0.10	0.01
”	921.0	0.21(3)	0.05(5)			22	19	0.31	-0.04
”	1062.4	0.16(2)	0.02(1)			6	4	0.14	0.03
536.1	1127.3	-0.02(4)	0.04(4)	16	14	17	16	-0.07	0
965.2	108.9	-0.01(4)	0.05(6)	11	9	7	6	-0.07	0
”	252.9	0.14(6)				19	17	0.11	0.01
”	423.6	0.10(2)	-0.05(3)			9	7	0.10	0.01
”	436.6	0.15(2)	0.03(2)			2	0	0.16	0.06
”	536.1	0.16(4)	-0.04(4)			16	14	0.11	0.01
”	691.8	0.14(2)	-0.05(3)			4	2	0.12	0.02
”	921.0	0.17(3)	-0.08(6)			22	19	0.19	-0.01
”	1062.4	0.12(2)	0.02(1)			6	4	0.11	0.01
1127.3	423.6	-0.07(3)	-0.03(4)	9	7	9	7	-0.08	0
	536.1	-0.06(3)	-0.02(4)			16	14	-0.07	0

[a] The 598.3-keV transition was not evaluated due to the contamination of spectra by neutron-induced background.

TABLE IV. Assignment of calculated states to the experimental levels. The columns labelled *configuration* and *prob* show the two strongest configuration components of the calculated wavefunction and their probability.

I^π	E_{exp} (keV)	E_{calc} [a] (keV)	Δ [b] (keV)	configuration 1 π^{-1}	configuration 1 ν^{-1}	prob %	configuration 2 π^{-1}	configuration 2 ν^{-1}	prob %
0^+	0	70	70	$s^2_{1/2}$	$p^2_{1/2}$	12	$s^2_{1/2}$	$f^2_{5/2}$	10
2^+	437	598	161	$s^2_{1/2}$	$p_{1/2}f_{5/2}$	10	$s_{1/2}d_{3/2}$	$p^2_{1/2}$	6
4^+	1128	1343	215	$s^2_{1/2}$	$p_{3/2}f_{5/2}$	11	$s_{1/2}d_{3/2}$	$p_{1/2}f_{5/2}$	10
6^+	2191	2378	187	$s_{1/2}d_{3/2}$	$p_{3/2}f_{5/2}$	17	$s^2_{1/2}$	$f_{5/2}f_{7/2}$	8
5^-	2263	2258	-5	$s_{1/2}h_{11/2}$	$p^2_{1/2}$	13	$s_{1/2}h_{11/2}$	$f^2_{5/2}$	11
7^-	2300	2272	-28	$d_{3/2}h_{11/2}$	$p^2_{1/2}$	10	$d^2_{3/2}$	$p_{1/2}i_{13/2}$	9
9^-	2723	2762	+38	$s^2_{1/2}$	$f_{5/2}i_{13/2}$	21	$d^2_{3/2}$	$f_{5/2}i_{13/2}$	15
11^-	3689	3655	- 34	$s_{1/2}d_{3/2}$	$f_{5/2}i_{13/2}$	46	$d^2_{3/2}$	$f_{5/2}i_{13/2}$	12
12^+	4287	4297	+9	$s_{1/2}h_{11/2}$	$p_{1/2}i_{13/2}$	44	$d_{3/2}h_{11/2}$	$p_{1/2}i_{13/2}$	15
14^+	4389	4374	-16	$d_{3/2}h_{11/2}$	$p_{1/2}i_{13/2}$	45	$s_{1/2}h_{11/2}$	$f_{5/2}i_{13/2}$	23
16^+	4925	4868	-58	$d_{3/2}h_{11/2}$	$f_{5/2}i_{13/2}$	89	$d_{5/2}h_{11/2}$	$f_{5/2}i_{13/2}$	4
15^+	5124	4979	-146	$s_{1/2}h_{11/2}$	$f_{5/2}i_{13/2}$	71	$d_{3/2}h_{11/2}$	$f_{5/2}i_{13/2}$	17
16^-	5916	5837	-80	$h^2_{11/2}$	$p_{1/2}i_{13/2}$	72	$d_{3/2}h_{11/2}$	$i^2_{13/2}$	10
17^-	6052	6069	+16	$h^2_{11/2}$	$p_{1/2}i_{13/2}$	47	$h^2_{11/2}$	$f_{5/2}i_{13/2}$	25
17^-	6162	6281	+119	$s_{1/2}h_{11/2}$	$i^2_{13/2}$	40	$d_{3/2}h_{11/2}$	$i^2_{13/2}$	23
18^-	6258	6128	-130	$s_{1/2}h_{11/2}$	$i^2_{13/2}$	77	$d_{3/2}h_{11/2}$	$i^2_{13/2}$	14
19^-	6305	6294	-12	$h^2_{11/2}$	$f_{5/2}i_{13/2}$	49	$d_{3/2}h_{11/2}$	$i^2_{13/2}$	46
22^+	7226	7262	+35	$h^2_{11/2}$	$i^2_{13/2}$	100			

[a] The binding energies are relative to the ground state of ^{208}Pb, but with the measured energy of the ^{204}Hg ground state set to zero (see text for details).

[b] The average linear/quadratic deviation for all states is +19 /100 keV. Considering only the states from 5^- upwards, the deviations are -21/69 keV.

TABLE V. Difference between calculated and measured binding energies for nuclei with various number of holes relative to ^{208}Pb for ground states and levels with the highest possible angular momentum that can be generated from the valence holes.

Nucleus	state	ΔE (keV)	state I^{π}	ΔE (keV)
^{205}Tl	ground state	+18	$35/2^{-}$	+5
^{204}Tl	ground state	+102	22^{-}	+12
^{204}Hg	ground state	+70	22^{+}	+35
^{203}Hg	ground state	+85	$53/2^{+}$	+20

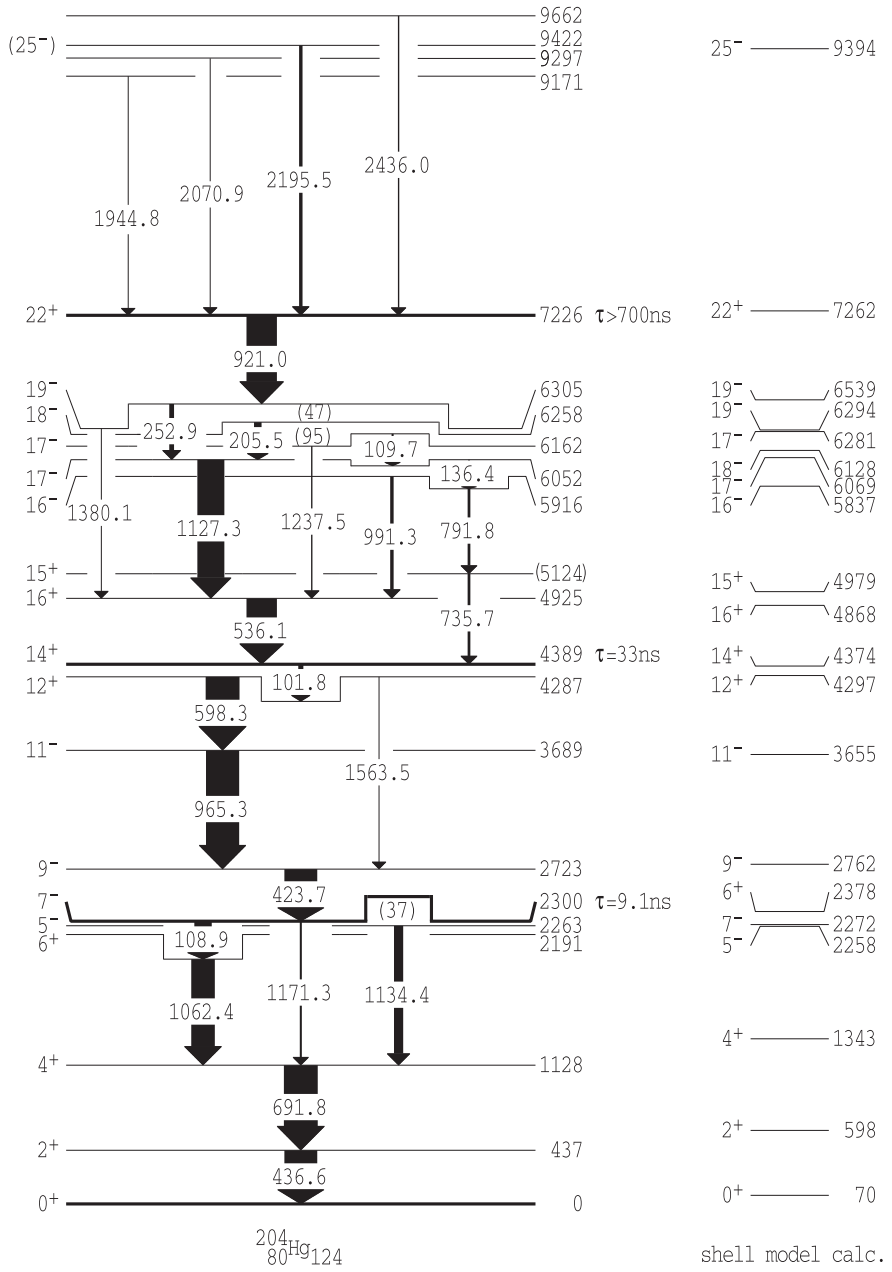

FIG. 2. Level scheme established for ^{204}Hg in the present work; the widths of the arrows correspond to the relative γ-ray intensities in the out-of-beam time region. The ordering of the 735.7- and 791.8-keV lines is not determined; therefore, the 15^+ state could also be located at 5180 keV. A comparison with shell-model calculations is presented on the right-hand side of the figure. The energy of the 25^- state located in this column is from an estimate based on the energy of the octupole phonon presented in the text and does not result from the shell model calculations. Spin and parity assignments are discussed in the text.

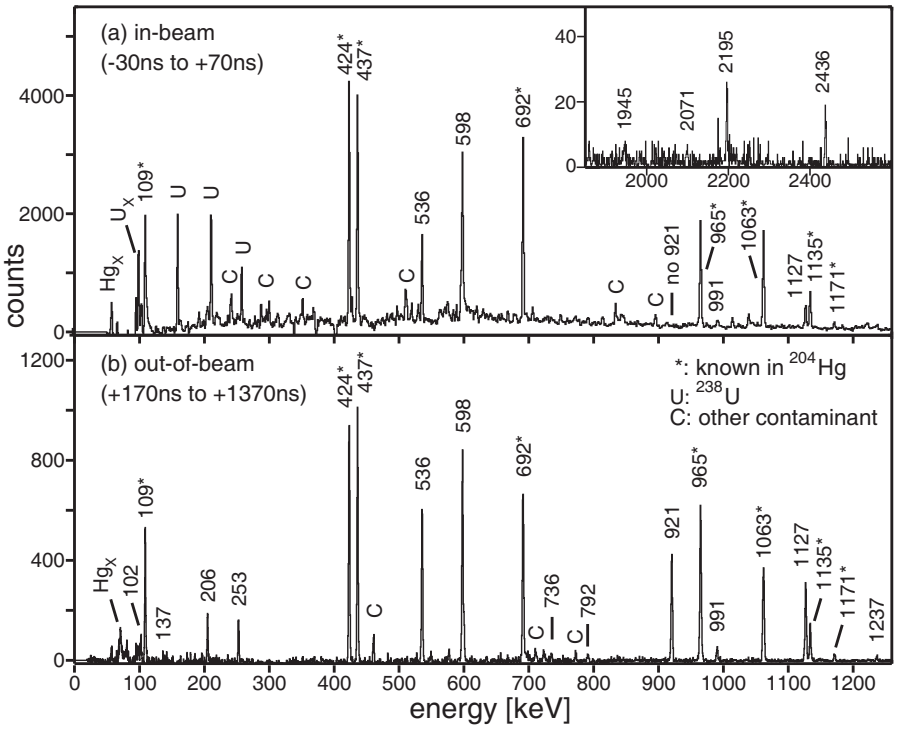

FIG. 3. Representative coincidence spectra, double-gated on specific γ rays, but with additional absolute time constraints, illustrating the main deexcitation paths in ^{204}Hg. Transitions labelled by energy are assigned to ^{204}Hg with those known previously marked with asterisks. Contaminant transitions from the strongly Coulomb-excited ^{238}U target are labelled with the letter "U", while other known contaminants are labelled "C". The two panels give (a) a sum of 28 spectra from the prompt coincidence cube gated on the the time region from -30 to $+70$ ns around the beam pulse, and (b) a sum of 43 spectra from the out-of-beam coincidence cube gated on the time region from $+170$ to $+1370$ ns after the beam pulse. The inset to (a) provides the high-energy part of the spectrum of in-beam γ rays observed 30-800 ns early with respect to the same 43 pairs of γ rays used to construct the spectrum in (b). Hence, this reveals transitions feeding the long-lived isomer at the top of the level scheme.

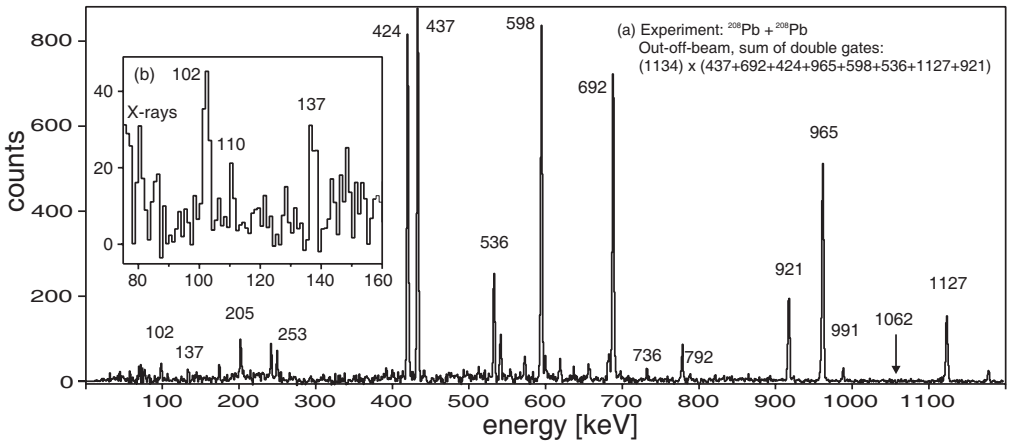

FIG. 4. Sum of out-of-beam, double-gated spectra from the ^{208}Pb+^{208}Pb experiment with gates as indicated in the figure, selected to observe the 110-keV line. The ten times stronger 108.9-keV transition is excluded by the coincidence requirement with the parallel 1134-keV line, as evidenced by the absence of the 1062.4-keV γ ray in this spectrum.

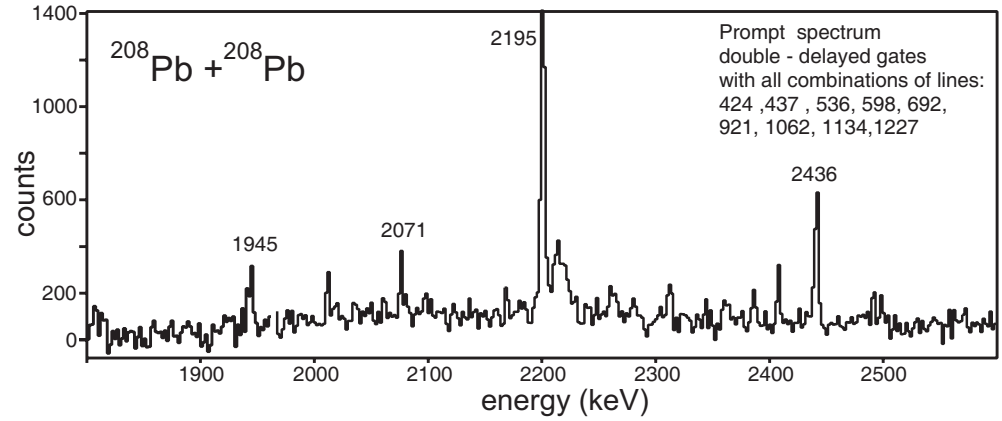

FIG. 5. Prompt spectrum obtained by summing the delayed double-gates on all combinations of strong lines below the 22^+ isomer. The γ rays marked with energies are prompt feeding transitions into the long isomer in ^{204}Hg, as confirmed by the coincidence relationships.

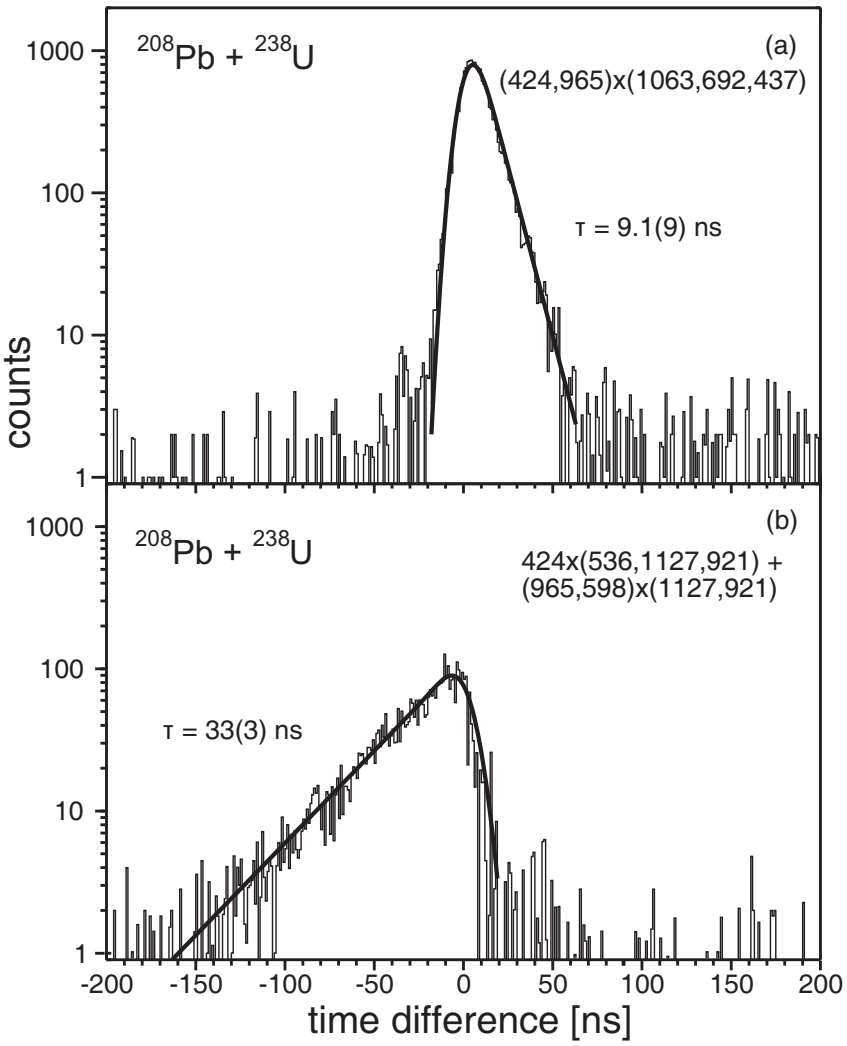

FIG. 6. Sums of spectra showing the time difference between the marked pairs of γ rays; (a) the measured lifetime of the 7^- isomer is $\tau = 9.1(9)$ ns, in agreement with the previous measurement of $\tau = 9.9(5)$ ns [13]; (b) a new isomer at 4389 keV with a lifetime of $\tau = 33(3)$ ns.

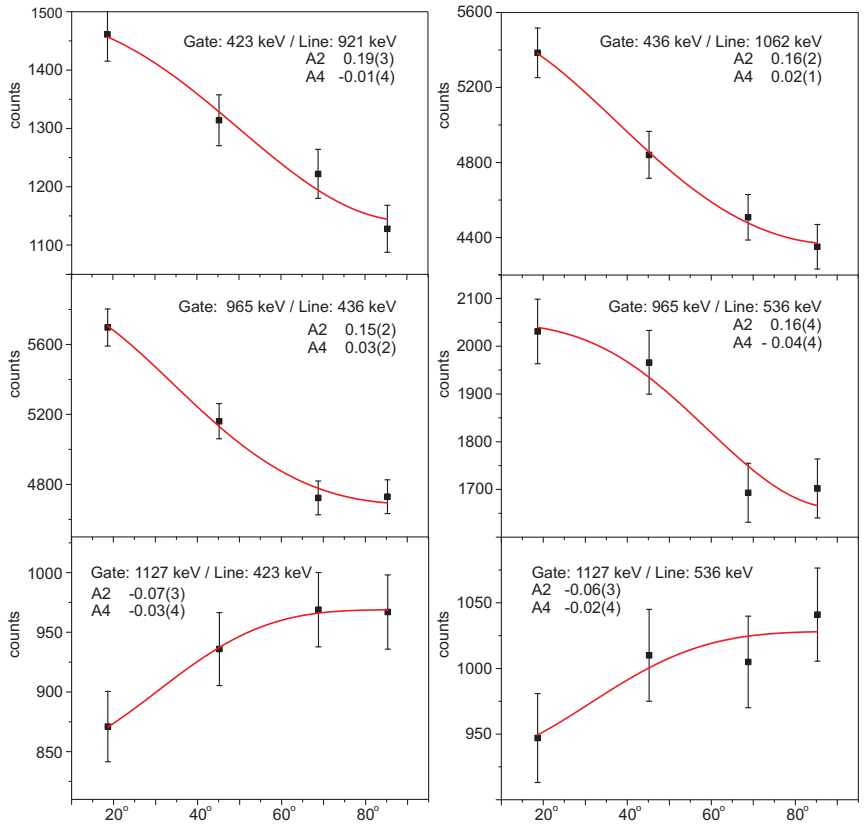

FIG. 7. Examples of angular correlations obtained for several transition pairs; the solid curves represent the fit to the data (see text for details).

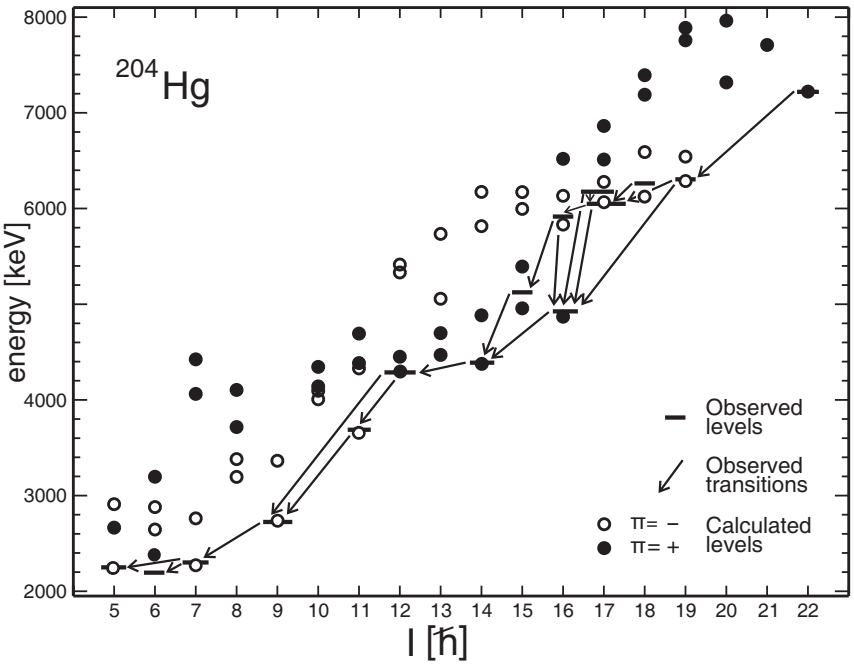

FIG. 8. Results of the shell-model calculations shown for ^{204}Hg from the 5^- state and up, with the energies of the two lowest calculated levels given for each spin and parity. The horizontal lines and the arrows indicate the observed levels and transitions, respectively.